Nano Energy 102 (2022) 107625

Contents lists available at ScienceDirect

Nano Energy

journal homepage: www.elsevier.com/locate/nanoen

Self-powered, high sensitivity printed e-tattoo sensor for unobtrusive arterial pulse wave monitoring

Mika-Matti Laurila [a,*], Mikko Peltokangas [b,c], Karem Lozano Montero [a], Jarmo Verho [b], Mira Haapala [b,c], Niku Oksala [b,c,d], Antti Vehkaoja [b,c], Matti Mäntysalo [a]

[a] Faculty of Information Technology and Communication Sciences, Tampere University, 33720 Tampere, Finland
[b] Faculty of Medicine and Health Technology, Tampere University, 33720 Tampere, Finland
[c] Finnish Cardiovascular Research Center, Tampere University, 33520 Tampere, Finland
[d] Vascular Centre, Tampere University Hospital, 33520 Tampere, Finland

ARTICLE INFO

Keywords:
Piezoelectric polymer sensors
P(VDF-TrFE)
Arterial pulse wave measurement
Additive fabrication
Electronic tattoo devices
Determination of direct piezoelectric coefficients

ABSTRACT

Self-powered, highly unobtrusive, low-cost and accurate arterial pulse wave monitoring devices need to be developed to enable cost-efficient monitoring of entire cardiovascular disease risk groups. We report the development of a scalable fabrication process for a highly unobtrusive piezoelectric ultra-thin (t ~ 4,2 μm) e-tattoo arterial pulse wave sensor which utilizes only transparent and biocompatible polymer-based materials. The ferroelectric performance of the ultra-thin P(VDF-TrFE) material layer is optimized through the use of crosslinked PEDOT:PSS electrodes; this results in ~70 % and ~34 % improvements in remanent polarization (P_r) and coercive field (E_c), respectively, when compared to the sensors with pristine PEDOT:PSS electrodes. The ultra-thin form factor enables access to the high bending mode sensitivity of the P(VDF-TrFE) material layer; the maximum sensitivity value achieved in uniaxial and multiaxial bending is ~1700 pC N^{-1}, which is ~50 times higher than the measured normal mode sensitivity. The increased sensitivity is linked to a specific set of direct piezoelectric coefficients using combination of experimental results, statistical analysis and finite element modeling. Finally, the accuracy of the e-tattoo sensor is demonstrated in the non-invasive measurement of radial artery pulse wave by comparing the signal to that obtained with reference device from 7 study subjects.

1. Introduction

Cardiovascular diseases are the most common cause of death in the world (17.9 million deaths in 2016) [1]. A significant portion of the deaths caused by the cardiovascular diseases could be prevented by developing affordable and easy-to-use detection methods for cost-effective screening of the risk population. Recently, the aortic pulse wave has emerged as a potential candidate for detecting various manifestations of cardiovascular diseases (e.g. coronary artery disease, cerebrovascular disease, hypertension) [2,3]. Because the aortic pulse wave can be reconstructed from peripheral pulse wave using generalized transfer functions, it should be possible to find the same markers from the peripheral arteries (i.e. radial artery at the wrist, or carotid artery at the neck) [3,4]. In current clinical practice, non-invasive pulse wave (PW) measurement from the radial/carotid artery is based on ultrasonic PW imaging or applanation tonometry [5,6]. However, neither of those methods are suitable for continuous monitoring of the risk population because they require a professional operator, are too expensive, and the devices are not wearable.

To address these issues, it has been proposed that the PW signal could be measured from the minute skin deformation caused by the pulsating radial/carotid artery located directly underneath the dermis using ultra-thin sensors. So far, such devices have been proposed based on various operating principles: capacitive [8,14], piezoresistive [9,12,16], piezoelectric [7,11,15,17], ultrasonic [11] and bioimpedance [13] (see Table 1). However, capacitive, piezoresistive, ultrasonic, and bioimpedance sensors require an external energy source for signal generation, which is problematic for on-skin bio-signal monitoring applications with limited energy supply. In contrast, utilization of the piezoelectric effect leads to energy-autonomous signal generation thereby limiting the energy consumption of the device. Despite the very promising results presented in abovementioned studies, there are certain drawbacks which need to be overcome to enable wider adoption of ultra-thin sensors for pulse wave monitoring. One of the main

* Corresponding author.
E-mail address: mika-matti.laurila@tuni.fi (M.-M. Laurila).

https://doi.org/10.1016/j.nanoen.2022.107625
Received 15 March 2022; Received in revised form 23 June 2022; Accepted 21 July 2022
Available online 3 August 2022

shortcomings has been that they often do not validate the obtained PW signal using a reference device, which makes it difficult to estimate the accuracy of the sensor [7,8,10,12–16]. Another issue is related to the loose definition of the term "ultra-thin": in certain cases, the total thickness of the device can be tens [7–9,16] or even hundreds of microns [11,14]. This limits the unobtrusiveness of the device and makes it questionable if the sensor can measure the signal accurately from the minute skin deformation caused by the pulsating artery without the use of a cuff. An additional shortcoming is related to the scalability of the fabrication process which has a direct impact on the affordability of the PW-sensors. Most of the devices utilize multi-step fabrication processes which are difficult to scale up (e.g. photolithography, evaporation, laser lift-off) [7,15], whereas readily scalable fabrication technologies (e.g. printing) are required for the fabrication of affordable sensors, and to enable cost-effective mass screening of the whole cardiovascular disease risk population consisting millions of potential patients.

Clearly, there is a need to further develop unobtrusive and affordable PW-sensors with minimal energy consumption and to study their accuracy in more depth. In this article, we address these issues through the development of a fully printed ultra-thin piezoelectric e-tattoo PW-sensor. The ultra-thin form factor (overall device thickness ~4,2 μm) enables the sensor to bend during the arterial PW-measurement leading to higher device sensitivity: the bending mode sensitivity is characterized in uniaxial and multiaxial modes and it is shown that the bending mode sensitivity of ~1700 pC N^{-1} is significantly higher when compared to the measured normal mode sensitivity of 31 pC N^{-1}; we are able to relate the high bending mode sensitivity to a specific set of direct piezoelectric coefficients using a combination of experimental results, finite element modeling and statistical analysis. As an additional benefit, the ultra-thin form factor enables conformable sensor attachment to skin and maximizes the device transparency, which results in a highly unobtrusive user experience necessary for continuously worn on-skin devices. We further show that the high sensitivity bending mode can be accessed in pulse wave measurement either by placing the ultra-thin sensor on the superficial artery at distal antebrachium without a cuff or by using a soft elastomer (PDMS) as a cuff. Finally, the accuracy of the PW-signal obtained with the proposed sensor is validated by comparing it to a PW signal measured simultaneously with a state-of-the-art reference device. The proposed sensors are the thinnest fully printed piezoelectric sensors reported so far. Furthermore, a comparison of corresponding ultra-thin sensors in Table 1 (i.e. references [15,17]) reveal that the sensors have the highest sensitivity value of any reported ultra-thin piezoelectric sensor.

2. Results

2.1. Fabrication process

The fabrication process for the ultra-thin e-tattoo sensor is illustrated in Fig. 1a. A glass carrier is spin-coated with a poly(trifluoroethylene) release layer followed by chemical vapor deposition of ~615 nm layer of Parylene-C. The Parylene-C layer acts as a substrate during the device fabrication and provides electrical and environmental insulation once the device is released from the glass carrier and attached to the skin. A 100:1 mixture of poly(3,4-ethylenedioxythiophene):poly (styrenesulfonate) (PEDOT:PSS) and (3-glycidyloxypropyl)trimethoxysilane (GOPS) (Fig. 1b) is inkjet printed onto the Parylene-C substrate to form the bottom electrode of the piezoelectric sensor. The GOPS improves the chemical and humidity stability of the PEDOT:PSS through cross-linking of the polymer structure [20–22], prevents the possible degradation of the PEDOT:PSS by the polar solvent (trimethyl phosphate, 2.8 D) of the poly(vinylidenefluoride-trifluoroethylene) (P (VDF-TrFE)) piezoelectric layer, and improves the ferroelectric performance of the ultra-thin P(VDF-TrFE) layer through reduction of leakage current (see next chapter). The effect of crosslinker on the conductivity of the PEDOT:PSS was minimized by keeping the GOPS content low at 1 vol %. According to previous study [22], this should lead to only ~13 % drop in the conductivity when compared to pristine PEDOT:PSS samples. The P(VDF-TrFE) solution is bar coated onto the bottom electrode resulting in straightforward and accurate control of the film thickness [17]; average dry thickness of the ultra-thin and thick sample sets were (3,6 ± 0,3) μm (total device thickness of only ~ 4,2 μm, Fig. 1 g) and (15,9 ± 0,6) μm (total thickness ~16,5 μm), respectively. The top electrode is inkjet printed onto the P(VDF-TrFE) using the same process/materials as for the bottom electrode. Piezoelectric behavior of the P (VDF-TrFE) is induced by in-situ poling the material with a high electric field of 90 V/μm (Fig. 1c). Finally, a temporary tattoo paper is used to facilitate easy transfer of the ultra-thin device from the glass carrier onto the skin [23], while the thin adhesive layer of the tattoo paper is used to improve the mechanical coupling between the skin and the device. This enables the utilization of the high bending mode sensitivity of the P (VDF-TrFE) in the measurement of the arterial pulse wave signal

Table 1
Ultra-thin PW sensors reported in the literature. Please note that it is not possible to report the same sensitivity units for all sensors because of varying operating principles and/or the lack of data necessary for transforming the units.

Reference	Year	Operating principle	Fabrication method	Sensor thickness (including substrate) (μm)	Sensitivity	Pulse wave signal validation	Number of PW test subjects
This work	2021	Piezoelectric	Inkjet / blade coating	4,2	1703 pC N^{-1}	Reference device	7
[17]	2021	Piezoelectric	Inkjet / blade coating	7	~38 pC/N †	Reference device	1
[16]	2021	Piezoresistive	Inkjet / blade coating	~40	0,99 kPa^{-1}	No	1
[15]	2020	Piezoelectric	Evaporation / spin coating	2,5	1300 pC N^{-1}	No	1
[14]	2020	Capacitive	Electrospinning / spray coating / lamination	~100	1,12 kPa^{-1}	No	1
[13]	2019	Bioimpedance	Spin coating / etching / cutting	< 1 ††	N/A	No	1
[12]	2019	Piezoresistive	Photolithography	N/A	1360 ‡	No	1
[11]	2018	Ultrasonic	Spin coating / laser ablation	240	N/A	Reference device	1
[10]	2017	Piezoelectric	Laser lift off / lamination / evaporation	~8 ††	0018 kPa^{-1}	No	1
[9]	2016	Piezoresistive	Evaporation / lamination	> 50 ††	0585 kPa^{-1}	Reference device	N/A
[8]	2015	Capacitive	Evaporation / lamination	36 ††	0,58 kPa^{-1}	No	1
[7]	2014	Piezoelectric	Photolithography + transfer printing	~25	~0005 Pa §	No	1

†Calculated based on sample capacitance (51.1 pF) and voltage sensitivity (749,1 mV/N)
††Estimated based on available data in the article (e.g. cross-section images, individual layer thicknesses)
‡ Gauge factor GF = $\Delta R/(R_0\varepsilon)$ where ε is the strain (%)
§Authors apparently mean detection limit, sensitivity not disclosed

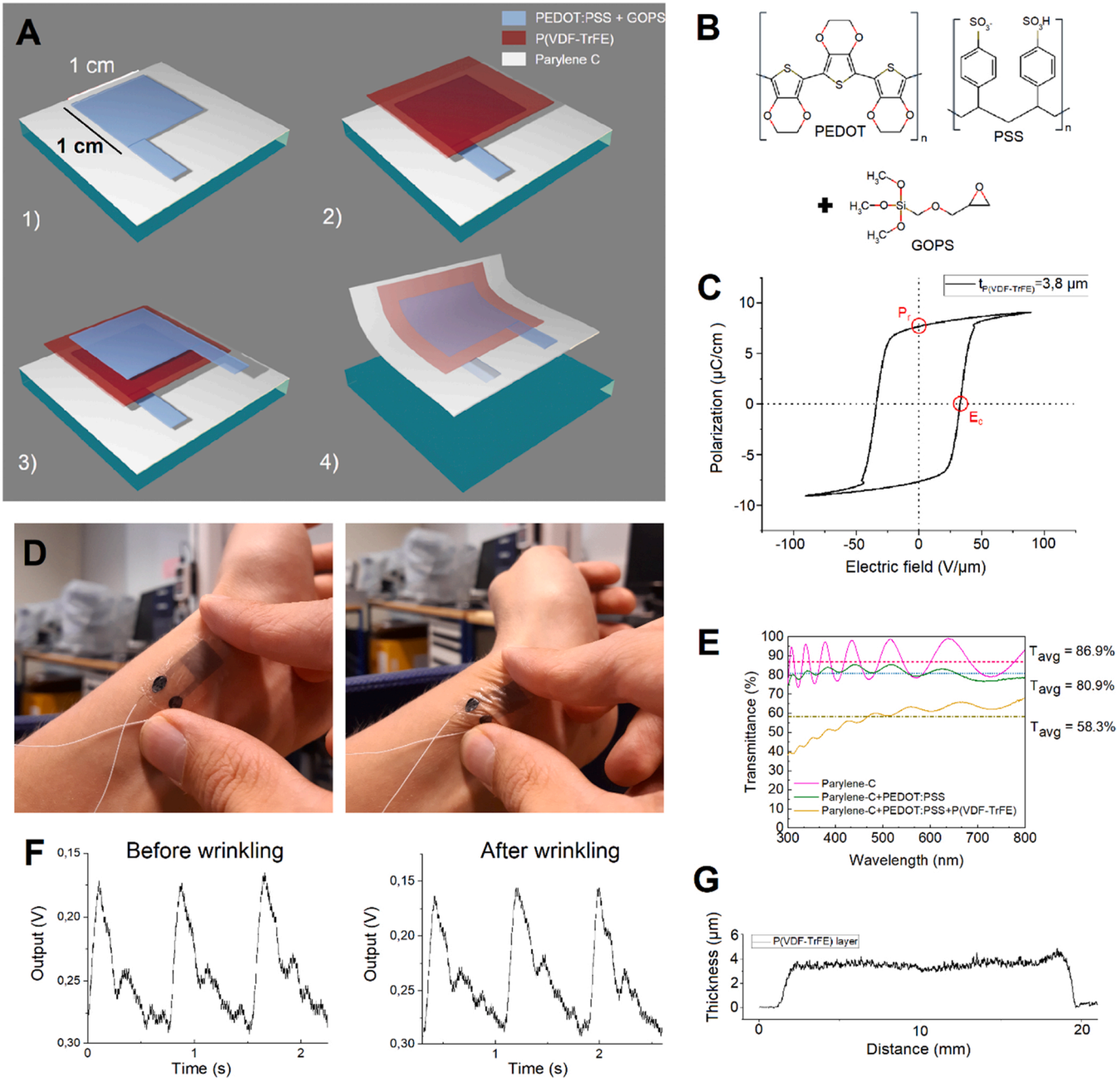

Fig. 1. : A) Fabrication process for ultra-thin sensor: 1) inkjet printing of PEDOT:PSS bottom electrode on Parylene-C substrate on glass carrier; 2) bar coating of P(VDF-TrFE) electroactive layer; 3) inkjet printing of PEDOT:PSS top electrode and 4) peel-off from the glass carrier. B) Chemical structures of PEDOT:PSS and GOPS cross-linker. C) Typical PE-loop for the ultra-thin sensor with points of remanent polarization (P_r) and coercive field (E_c) indicated. D) Sensor attached on top of the radial artery at distal antebrachium without/with wrinkling. E) Transmittance of sensor. The Swanepoel method was used to calculate the Parylene-C thickness from the transmittance graph (see SI and **Fig. S 1**) F) Arterial pulse waves measured before and after wrinkling the sensor. G) Thickness of typical P(VDF-TrFE) layer from the ultra-thin sample set.

(Fig. 1 f). Once attached to the skin (Fig. 1d), the device is highly unobtrusive not only because of its thickness and lightweight, but also because of its transparency (Fig. 1e): in the visible light spectrum (300–800 nm) the average transmittance of ultra-thin sample is 58,3 %.

2.2. *Optimized ferroelectric performance of ultra-thin P(VDF-TrFE) films with GOPS crosslinked PEDOT:PSS electrodes*

Polarization-electric field hysteresis loop (PE-loop) measurement was performed to demonstrate that the ultra-thin P(VDF-TrFE) layer exhibits sufficient ferroelectric performance. In the PE-loop measurement a high electric field (E) is applied over the thickness of the P(VDF-TrFE) while measuring the polarization (P). The average saturated PE-loops for ultra-thin P(VDF-TrFE) layers utilizing pristine (PEDOT:PSS pristine) and crosslinked PEDOT:PSS electrodes (PEDOT:PSS GOPS) are shown in Fig. 2a. The samples with GOPS crosslinked PEDOT:PSS exhibit clear ferroelectric hysteresis with average remanent polarization (P_r, Fig. 1c) of (7,5 ± 0,2) µC/cm^2 and average coercive field (E_c, Fig. 1c) of (46,9 ± 8,1) V/µm, which correspond closely to literature values for P(VDF-TrFE) (i.e. P_r = 6–8 µC/cm^2 and E_c = 40–60 V/µm [18,19]). Samples with GOPS crosslinked PEDOT:PSS bottom electrodes were also compared to samples with metal based (Ag)

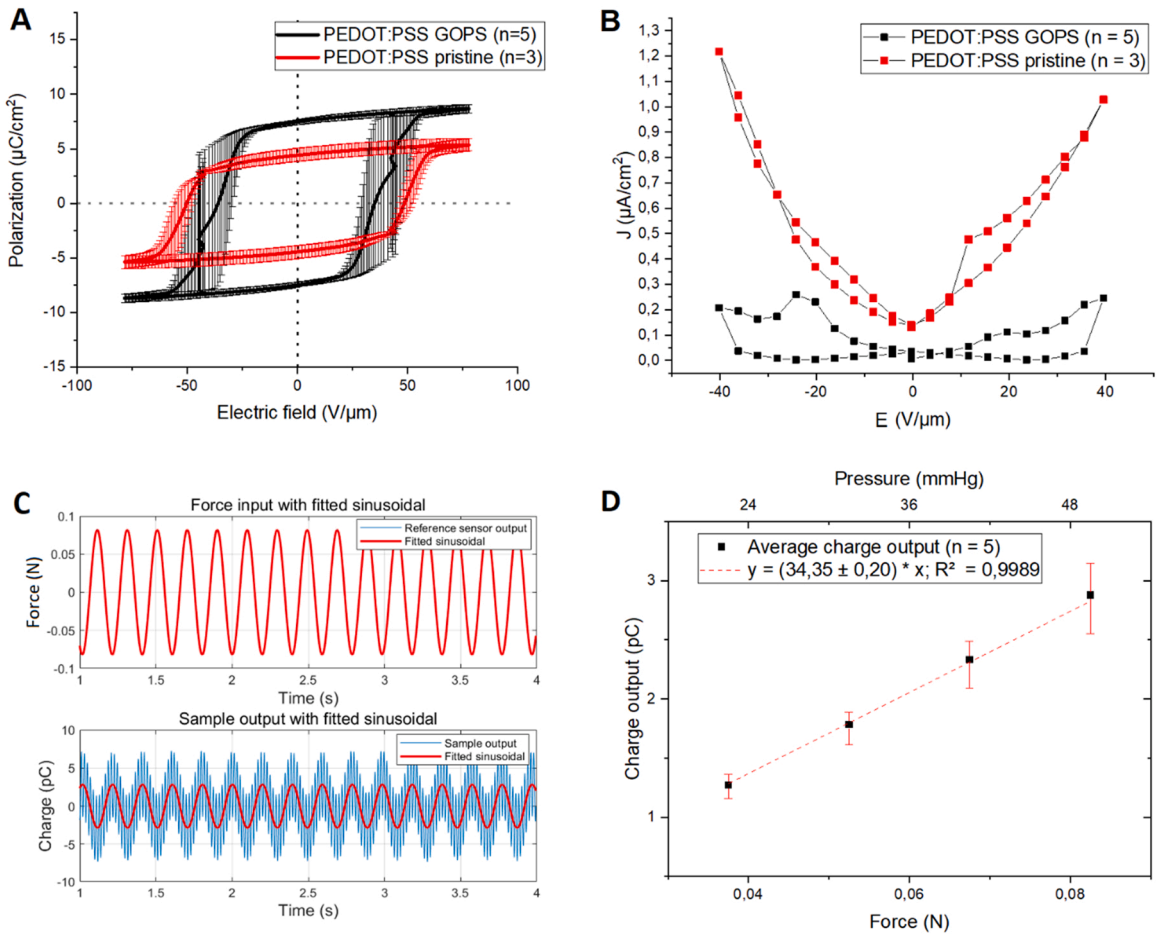

Fig. 2. : A) PE-loops for P(VDF-TrFE) based ultra-thin e-tattoo sensors (P(VDF-TrFE) thickness ≈ 3,6 μm) with GOPS crosslinked and pristine PEDOT:PSS electrodes. The error bars indicate the range of measurements. B) Leakage current density for P(VDF-TrFE) film with GOPS crosslinked and pristine PEDOT:PSS electrodes. Each data point is the average of measured samples. C) Typical measurement result used in calculation of normal mode sensitivity: Matlab was used to fit sinusoidal functions to the output of the dynamic force reference sensor (above) and the output of the sensor (below) and the normal mode sensitivity (or $d_{33.eff}$) can be calculated as the ratio of the two. Note that in the upper graph, dynamic force reference sensor output and fitted sinusoidal are overlapping completely. D) Linearity of the sensor output in the dynamic pressure range of the arterial pulse wave. The constant of the fitted linear function corresponds to the average normal mode sensitivity value over the measured pressure range.

bottom electrodes as these provide a reference point for the ferroelectric performance of the P(VDF-TrFE) (see SI). The close match between both PE-loops (see **Figure S 3**) indicates that the GOPS cross-linked PEDOT:PSS provides optimized performance of the P(VDF-TrFE). The main advantage of cross-linked PEDOT:PSS over the metal electrode materials is its transparency which enhances the unobtrusiveness of the sensor.

The use of GOPS crosslinked PEDOT:PSS electrodes leads to a significant improvement in the ferroelectric performance of the ultra-thin P(VDF-TrFE) layer. This is apparent by comparing the aforementioned PE-loops to those obtained from similar average P(VDF-TrFE) thickness samples (~3,6 μm) with pristine PEDOT:PSS electrodes (Fig. 2a): the average P_r value increased from 4,4 μC/cm^2 to 7,5 μC/ cm^2 (~70 %) and the average E_c value decreased from 56,5 V/μm to 42,2 V/μm (~34 %) through the addition of the crosslinker. This improvement is likely related to the order of magnitude lower leakage current density (J) in samples with crosslinked PEDOT:PSS electrodes (Fig. 2b) which leads to a higher effective field over the P(VDF-TrFE) film during the poling step (Fig. 2b) thereby improving the ferroelectric performance of the P(VDF-TrFE). In order to understand the mechanism behind the observed leakage current reduction, two common leakage current models, space charge limited current (SCLC) and Poole-Frenkel (P-F), were fitted to the measurements using linear regression and the fit of the models were compared [24–26] (see SI, especially Figure S4a and b). Based on the adjusted coefficient of determination (R^2) generated by the linear regression analysis (see legends in Figure S4a and b), both the SCLC and P-F models predict the data well for the samples with pristine PEDOT:PSS electrodes. In contrast, for cross-linked PEDOT:PSS electrodes, only the SCLC fits the data well whereas the P-F model fits the data very poorly. We can therefore conclude that the P-F type conduction is reduced by the addition of the crosslinker. As the P-F type conduction is related to the insulator trap states we hypothesize that the reduced leakage current is related to the improved chemical stability of the cross-linked PEDOT:PSS which prevents the leaching of the PEDOT:PSS in the P(VDF-TrFE) layer thereby preventing the creation of trap states.

2.3. Normal mode sensitivity

The P(VDF-TrFE) exhibits direct piezoelectric effect which can be employed in the measurement of arterial pulse wave. In traditional arterial tonometry, the sensor is attached on a rigid substrate which is then pressed against the artery [19]. The rigid substrate limits the possibility of bending of the sensor such that only deforming forces present in the piezoelectric layer are those normal to the sensor surface (i.e. compressive forces). This leads to the so-called normal mode sensitivity of the sensor, which is equal to the effective piezoelectric coefficient $d_{33.eff}$ of the piezoelectric material (see SI for the derivation of $d_{33.eff}$). The normal mode sensitivity / $d_{33.eff}$ measurement was performed on a rigid glass carrier in order to exclude possible bending of the device and to

limit the charge generation to the area of the force probe. Furthermore, the applied static and dynamic force were chosen so that the generated pressure corresponds approximately to the typical pressure range in the arterial pulse wave measurement i.e. ~ 40 mmHg dynamic and ~100 mmHg static pressure. The force input and charge output signals of a typical measurement are shown in Fig. 2c. The average normal mode sensitivity / $d_{33.eff}$ of 8 samples was (30,5 ± 2,7) pC N^{-1} which closely correspond to the P(VDF-TrFE) d_{33}-values reported in literature 25–35 pC N^{-1} [29,30]. In order to verify the linearity of the sensor output in the pulse wave dynamic pressure range, the charge output of a sensor sample was measured between 22,4 mmHg and 49,2 mmHg dynamic pressure (Fig. 2d), and linear regression was used to fit a line to the measured data. The regression analysis with R^2 = 99,89 % and a standard deviation of 0,20 indicates a high degree of linearity in the dynamic range of pulse wave signal.

2.4. Bending mode amplified sensitivity

In general, the bending deformation d of a material layer suspended between two supports is inversely proportional to the cube of the layer thickness h according to $d = L^3F/(4wh^3E)$, where L is the distance between supports, F the applied force, w the width of layer and E the Young's modulus of the material [31]. The ultra-thin form factor of the e-tattoo sensor should therefore maximize the bending deformation during arterial pulsation. Together with previously observed high bending mode sensitivity of various piezoelectric materials [7,32,33], this should enable pulse wave signal measurement from minute skin deformation on top of the artery. In cuffed pulse wave measurement, it should be possible to induce the bending mode by pressing the ultra-thin sensor against the artery with a soft elastomer. To test these hypotheses, uniaxial and multiaxial bending mode response were measured for ultra-thin e-tattoo sensors with ~3,9 μm and ~16,7 μm P(VDF-TrFE) thickness. Devices with similar P_r values (~7,2 μC/cm^2 for both, **Figure S 9**) were chosen to exclude the effect of sample-to-sample piezo-/ferroelectric performance variation.

In cuffless pulse wave measurement, the ultra-thin e-tattoo sensor will deform with the skin during arterial pulsation. In this situation, the deforming force is applied from underneath the sensor by the pulsating artery, and this will cause convex bending force on the ferroelectric layer. In order to test the performance of the sensor in such a situation, the sensor was attached to a PET sheet (t = 125 μm) with temporary tattoo adhesive and convex bending was induced using the previously described measurement system the sensitivity measurement system described in Materials and Methods with a cylindrical metal piece between the electrodynamically actuated force probe and the PET sheet (**Figure S 10**a). The sensor charge output is plotted as a function of applied force in Fig. 3a. The slope of the linear regression fit shows that reducing the thickness of the sensor leads to higher sensitivity in this deformation mode: the sensitivity for thick and thin samples are 1169,5 pC N^{-1} and 1713,8 pC N^{-1} (~46.6 % increase). Furthermore, the nearly

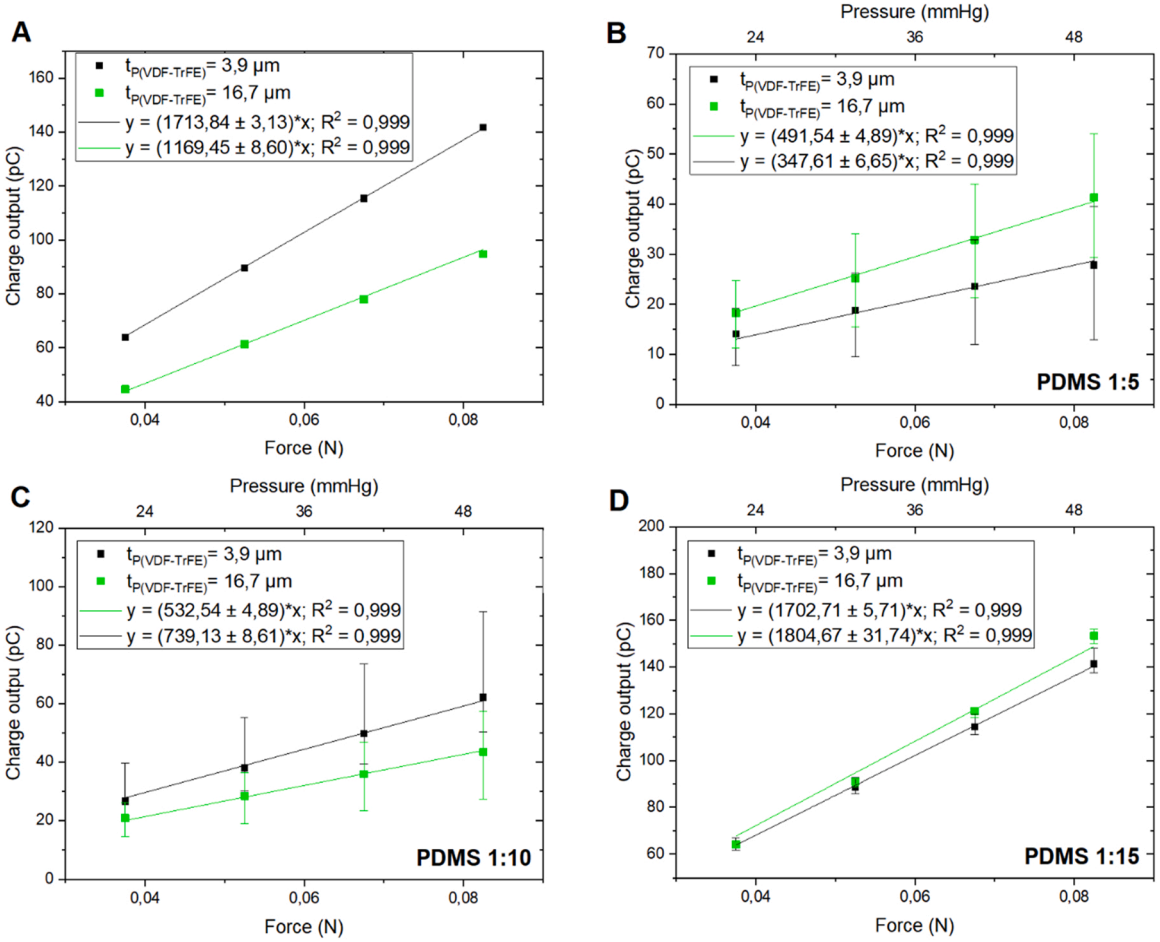

Fig. 3. : A) Linearity of the output of ultra-thin and thick sample in a convex bending mode in the dynamic pressure range of the pulse wave. The constant of the fitted linear function represents the average sensor sensitivity in this pressure range. The fitting was done using the average of five measurements. B) Output and linearity of the thick and thin sensor in multiaxial bending mode on substrate with 1:5 curing agent-to-DMS ratio. The constant of the fitted linear function represents the average sensor sensitivity in this pressure range. Fitting was done using the average of five measurements and error bars show the range of measurements. C) Same for 1:10 curing agent-to-DMS ratio. D) Same for 1:15 curing-agent-to-DMS ratio.

perfect fit of the linear function ($R^2 = 99{,}9$ %) indicates high linearity of sensor response in the dynamic pressure regime of the arterial pulse wave. It must be also noted that in traditional tonometry the induced forces are mostly normal to the sensor surface, and the sensor sensitivity is thus determined by the normal mode sensitivity / $d_{33.eff}$ which was $30{,}5 \pm 2{,}7$ pC N^{-1} for our sensors. Employing the uniaxial bending mode, and minimizing the sensor thickness, should therefore result in a ~50-fold increase in the sensitivity of the thin sample in the dynamic pressure range of the arterial pulse wave.

In cuffed pulse wave measurement, bending deformation can be induced in the P(VDF-TrFE) layer by pressing the sensor against the artery with a soft elastomer. Similar to cuffless measurement situation, the deforming force is applied from underneath the sensor by the pulsating artery; however, now the soft elastomer also provides back pressure which complicates the overall deformation by causing e.g. compressive forces to the P(VDF-TrFE) layer; i.e. the forces in this case are multiaxial. To characterize the sensor in such situation, it was attached on a poly(dimethylsiloxane) (PDMS) substrate while the charge output/sensitivity was characterized in the dynamic pressure range of the pulse wave using the measurement system described in Materials and Methods (Figure S 10b). The effect of the elastomer softness on sensitivity was investigated by varying the curing agent-to-DMS mixing ratio from 1:5–1:15 which corresponds to a decrease in Young's moduli from 1,6 GPa to 0,4 GPa (Figure S6–7). Based on Fig. 3b-d, it is apparent that the sensitivity is mainly affected by the softness of the substrate, with softer substrate resulting in higher sensitivity: as the substrate Young's moduli decreases from 1,6 GPa to 0,4 GPa, the sensitivity (i.e. slope of the fitted functions in Fig. 3b-d) of the thin and thick sample increases 4,9 and 3,7 fold, respectively. In contrast, the thickness of the P(VDF-TrFE) layer has a lesser effect: on average only a 6 % change in sensitivity is observed when the P(VDF-TrFE) thickness is increased from 3,9 to 16,7 μm. This shows that the ultra-thin sensor deformation and sensitivity are mainly determined by the mechanical properties of the soft elastomer substrate. The linearity of the sensor response in the dynamic pressure range of pulse wave is outstanding (R^2 = 99,9 %), because PDMS's stress-strain relationship is relatively linear in the said pressure range (Figure S 6–5). It must be noted, however, that at higher stresses the non-linear behavior of PDMS becomes apparent and the sensitivity vs. pressure relationship is best modeled by a polynomial fit (**Figure S 11**). The maximum multiaxial sensitivity of the thin sample was approximately 1700 pC N^{-1} (i.e. ~50 fold higher than the measured normal mode sensitivity) thereby indicating high potential for the bending based arterial pulse wave measurement.

$$\begin{bmatrix} & & d_{15} \\ & d_{24} & \\ d_{31} & d_{32} & d_{33} \end{bmatrix} = \begin{bmatrix} & & -36,3 \\ & -40,6 & \\ 1,0 & 6,9 & -34,9 \end{bmatrix} \; pC/N$$

2.5. Origin of high bending mode sensitivity of P(VDF-TrFE)

The piezoelectric effect is described by the piezoelectric constitutive equations (in strain-charge form and matrix notation):

$$\{S\} = [s^E]\{T\} + [d^t]\{E\} \quad (1)$$

$$\{D\} = [d]\{T\} + [\epsilon^T]\{E\} \quad (2)$$

where S describes the strain, T the stress, E the electric field, and D the electric displacement components; and where the $[s^E]$ is the compliance matrix under constant electric field, $[d^t]$ the transpose of the coupling matrix, $[d]$ the coupling matrix and $[\epsilon^T]$ the permittivity matrix under constant stress [34]. It is clear from above, that the sensitivity of the piezoelectric material is defined by the material parameters $[s^E]$, $[d]$ and $[\epsilon^T]$. However, $[s^E]$ and $[\epsilon^T]$ are not as strongly dependent on the processing conditions as the $[d]$, which in the case of P(VDF-TrFE) has been shown to be strongly affected by e.g. the poling process [35].

We, therefore, assume that the high bending sensitivity of the piezoelectric material arises mainly from a specific combination of direct piezoelectric coefficient values in the coupling matrix, and solving them would therefore provide a more thorough understanding of the origin of the high bending mode sensitivity of the P(VDF-TrFE). To accomplish this, we combine experimental sensitivity measurements with finite element (FE) modeling and statistical analysis (see Figure S5). Specifically, the method consists of: 1) experimental determination of the sample sensitivity in normal and multiaxial mode (results in previous chapters); 2) generation of FE models corresponding to each measurement situation (see S6.1); 3) using design of experiments method to generate a statistical model between the d-coefficients and FE-modeled sensor sensitivity (see S6.2 and S6.3); 4) optimizing the d-coefficients so as to correspond to the experimentally determined normal and multiaxial bending mode sensitivity values (see S6.4). The resulting optimized coupling matrix, which is responsible for the observed high bending mode sensitivity, was:

The FE model with an optimized coupling matrix was then used to predict the sensitivity of the e-tattoo sensor on various softness PDMS substrates (Fig. 4a). The FE-model predicted sensitivity on top of 1:5, 1:10 and 1:15 PDMS are 479 pC N^{-1}, 745 pC N^{-1} and 2006 pC N^{-1}, respectively. These correspond well with the experimentally measured values.

We also derive a simple statistical model to relate the sensitivity of the e-tattoo sensor to the softness of the substrate material. To accomplish this, the FE-model was first used to predict the normal mode sensitivity, and then the experimental and FEM predicted normal mode and multiaxial mode sensitivities were plotted as a function of the substrate Young's moduli (Fig. 4b); normal mode sensitivity was measured/modeled on Parylene-C substrate (E = 4,5 GPa [36]). The normal mode sensitivity represents the extreme case where there is no bending deformation during the measurement, and which therefore provides a boundary condition for the constant of the statistical model. Because the ultra-thin sensor sensitivity is mainly determined by the strain induced on the PDMS, which depends on the Young's modulus according to 1/E, the experimental and FEM data were fitted with a simple model of the form:

$$S = a \cdot \frac{1}{E^b} + d_{33.eff} \quad (3)$$

where S is the sensitivity; a and b coefficients; E the Youngs modulus of the substrate and $d_{33.eff}$ the effective piezoelectric constant measured on hard substrate (i.e. the normal mode sensitivity of the sensor). The model constants and coefficients are for as follows: $a_{exp} = 1{,}77 \cdot 10^{10} \pm 0{,}71 \cdot 10^{10}$, $b_{exp} = 1{,}25 \pm 0{,}03$, $d_{33.eff.exp} = 30{,}5$, and $a_{FEM} = 1{,}21 \cdot 10^{10} \pm 1{,}47 \cdot 10^{10}$, $b_{FEM} = 1{,}21 \pm 0{,}09$, $d_{33.eff.\ FEM} = 30{,}46$. The model predicts the experimentally determined and FE-modeled sensitivity values with high accuracy ($R^2 = 100$ % and $R^2 = 99{,}6$ %, respectively), thereby

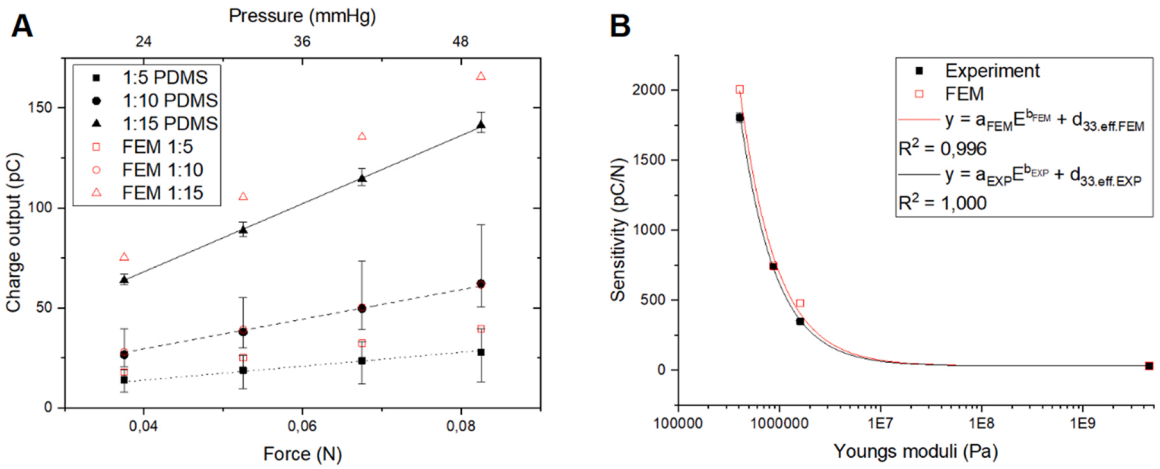

Fig. 4. A) Comparison of experimental and FE-model predicted sensitivity values of the ultra-thin sensor on different PDMS ratios. B) Measured and modeled sensitivity of the ultra-thin sample as a function of the substrate Young's moduli measured at constant dynamic pressure of 40,3 mmHg. The first six datapoints from the left are sensitivities measured/modeled on PDMS, while the rightmost data points (at E = 4,5 GPa) are the normal mode sensitivity measurement/modeling on Parylene-C substrate. The coefficients and constants of the fitted model are given in the text.

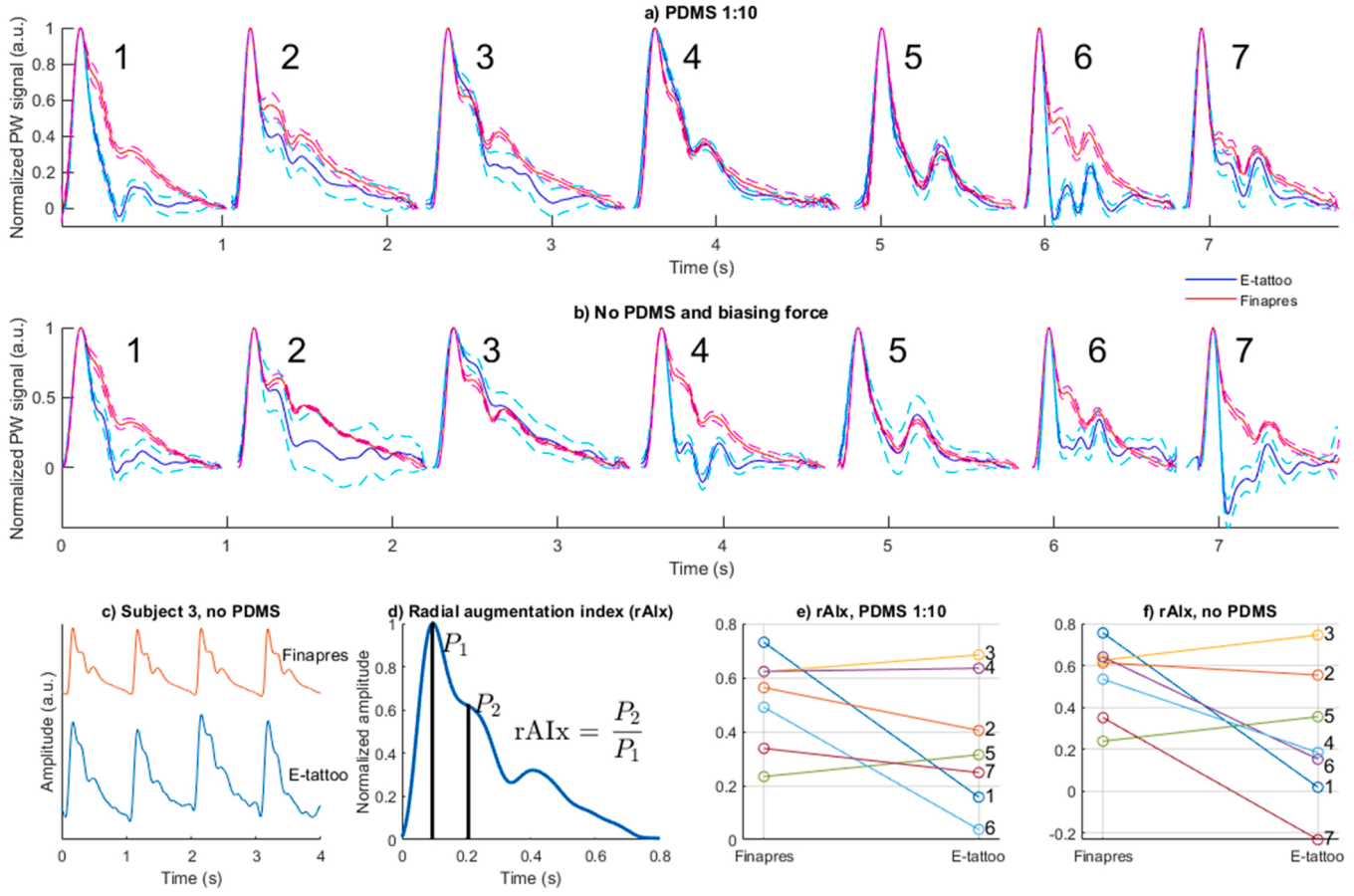

Fig. 5. a)-b) Comparison between the averaged e-tattoo sensor signal and reference signal recorded with Finapres NOVA in case of bias force provided with a 1:10 PDMS sheet and an elastic wristband on 7 test subjects (a) and with no PDMS and no bias force (b). The dashed lines show one standard deviation limits. c) Example of the concomitant signals from the reference and e-tattoo signal with no PDMS and no bias force. d) The definition of radial augmentation index rAIx. e)-f) Spaghetti plots on the value of rAIx based on the e-tattoo sensor signal and reference signal with 1:10 PDMS (e) and no PDMS and no bias force (f).

indicating that the sensitivity of the developed e-tattoo sensor is mainly affected by the mechanical properties of the substrate. It must be noted that the above model only applies for ultra-thin samples of < 20 μm thickness.

2.6. Arterial pulse wave measurement and analysis

The applicability of the proposed piezoelectric e-tattoo sensor for physiological measurements was tested in non-invasive arterial blood pressure pulse waveform measurements from the left distal radial artery and compared to the pulse waveform signal recorded with a reference device (Finapres NOVA) using a finger cuff located at the left index finger (Figure S12). In the experiments, the sensor was tested with no bias force as well as with the bias force provided using a wrist band and ~4 mm thick PDMS sheets with mixture ratios of 1:5, 1:10, and 1:15. Examples of results for 1:10 PDMS are shown in Fig. 5a) and b) as an average pulse waveform (continuous line) with one standard deviation limits (dashed line) for each test subject 1 – 7 for both e-tattoo sensor (blue) and reference device (red). An example of concomitant sensor signals is shown in Fig. 5c) from an experiment in which the e-tattoo sensor was placed on top of the radial artery without providing any bias force.

As seen in Fig. 5a) and b), the similarity between the e-tattoo sensor signal and the reference varies from subject to subject, as well as between the test conditions. There are occasional disturbances in the e-tattoo sensor signals due to its high sensitivity, which makes the waveform analysis of individual pulse waves not feasible in many cases. However, as seen in Fig. 5a) and b), averaging improves the signal-to-noise ratio considerably and results in good-quality and relatively similar waveforms, especially with 1:10 PDMS (Fig. 5a, test subjects 2 – 5 and 7). Almost equally good results were obtained with 1:5 PDMS. The waveforms are relatively similar with test subjects 2, 3, and 5 also when no bias force was applied (Fig. 5b). However, 1:15 provided the worst pulse-wave measurement results, despite the experimental and FE-modeling results clearly showing that the use of the softest elastomer should maximize the sensitivity. The likely cause for this contradictory result is that the mechanics of the test bench differ from the mechanics of the actual pulse wave measurement which is affected by, e.g., anatomy of the wrist.

Furthermore, the different measurement location causes some differences between the e-tattoo sensor and the reference signals, and relatively high lower cut-off frequency of the system causes in some cases rapid decrease in the e-tattoo sensor signal after its peak value and even complete differentiation of the signal as e.g. in case of test subject 6 with 1:10 PDMS (Fig. 5a) as well as test subject 7 when no bias force is applied (Fig. 5b). The missing low-frequency contents of the distorted e-tattoo sensor signals are also seen when comparing the power spectral density estimates of the e-tattoo and reference sensor signals (**Figure S 13**). The improper frequency response of the system in some experiments, such as in the case of test subject 4, is caused by insufficient mechanical coupling of the sensor. With test subject 4, adding the bias force with a thin PDMS-sheet and an elastic wrist band solved the problem (Fig. 5a) and b). On the other hand, the mechanical coupling is affected also by the exact placement of the sensor and small between-subject variations in the anatomy of the wrist [37].

In addition to the mechanical factors, the electrical characteristics of the system affect the frequency response. The lower cut-off frequency of a piezoelectric sensor connected to a non-inverting voltage amplifier is affected by the impedance of the sensor itself. This, in turn, is affected by the thickness of the P(VDF-TrFE) layer (Figure S14): as the layer thickness is decreased, the leakage resistance decreases faster than the capacitance increases, and the resulting lower cutoff frequency is therefore increased. This can be problematic for pulse wave measurements where low-frequency content is necessary for proper reproduction of the pulse wave signal. The frequency response variations could be compensated by adding an external capacitor in parallel with the sensor but its drawback, however, is the decreased sensitivity of the measurement system. Alternatively, it could be possible to increase the leakage resistance of the P(VDF-TrFE) with nanofillers such as ZnO [38] or surface-treated BaTiO3 and MWCNTs [39], while simultaneously having an even positive effect on the sensitivity [40].

Fig. 5d) presents the definition of radial augmentation index (rAIx) as a ratio of late (P_2) and early (P_1) systolic peaks as $rAIx = P_2/P_1$ [6,7,41], which provides information on the pressure augmentation in the arterial tree and thus the arterial stiffness and vascular health. The rAIx values presented in Fig. 5e) and f) are computed for the averaged waveforms: the figures show the spaghetti plot presentations for the rAIx values computed from the e-tattoo sensor signal and the reference signal for each test subject with the bias force provided through 1:10 PDMS as well as without bias force. With 1:10 PDMS cuffed e-tattoo sensor (Fig. 5e), the rAIx values compare well with the reference signal except in the case of test subjects 1 and 6 with clearly distorted pulse waveforms (2-tailed Wilcoxon signed-rank test: $p \approx 0.81$ if test subjects 1 and 6 are excluded, and $p \approx 0.22$ if included). In addition, problems with the mechanical coupling due to missing bias force increase the high-pass cut-off frequency of the system and thus decrease the value of rAIx especially with test subjects 1, 4, 6, and 7 compared to the reference and 1:10 PDMS situation, but still the rAIx values are at the same level in the successful measurements (2-tailed Wilcoxon signed-rank test: $p \approx 0.50$ if the test problematic subjects 1, 4, 6, and 7 are excluded; $p \approx 0.63$ if only test subjects 1 and 6 are excluded as in case of 1:10 PDMS; and $p \approx 0.16$ if all the test subjects are included). Even though our sample size is relatively small, it is still larger than in many other similar studies [7,17] Our results show that it is possible to measure a radial artery pulse wave with a fully-printed piezoelectric e-tattoo sensor and determine the value of the rAIx accurately enough also without any supporting bias force. Despite these results, challenges with the requirement of extremely low high-pass cut-off frequency and mechanical coupling are present.

2.7. Mechanical durability of the sensor

In order to check the durability of the sensor, 110 Hz cyclic loading was applied to a sample fabricated over a year ago for approximately three hours while simultaneously measuring its output voltage. The test was conducted in a controlled environment using a peak-to-peak dynamic force of 0.25 N. The output voltage remained stable for the whole duration of the test i.e. 1188000 cycles (see Figure S15). Considering that the average pulse rate of a human is approx. 80 beats/min, this would equal to cyclic loading during a 10 day long pulse wave measurement. It must be noted however that in long term wearing the body will also secrete sweat which may affect the performance of the sensor despite the protective Parylene-C layer between the skin and the piezoelectric material, and the use of cross-linked PEDOT:PSS as electrode material.

3. Discussion

We have reported a facile printing-based fabrication method for an e-tattoo type ultra-thin arterial pulse wave sensor. Crosslinking of the PEDOT:PSS electrodes leads to significant improvement in the ferroelectric performance of the ultra-thin P(VDF-TrFE) layer (~70 % improvement in P_r value and ~34 % improvement in E_c value). Minimized sensor thickness enables access to the high uni-/multiaxial bending mode sensitivity of the P(VDF-TrFE) which are up to 50-times higher than the normal mode sensitivity; a FEM model for the sensor was generated to corroborate these results. Cuffless and soft-elastomer cuffed pulse wave measurements were performed using the e-tattoo sensor. Comparison to reference device with $n = 7$ test subjects shows that best match in pulse waveform derived clinically relevant radial augmentation index is achieved with soft elastomer cuff with intermediate Young's modulus (1:10 PDMS) ($p \approx 0.22$ with all the test subjects,

$p \approx 0.81$ with 5 measurements with no problems). Cuffless measurement is also possible with the e-tattoo sensor even though the experiment-to-experiment variation is significant due to challenges with the mechanical coupling of the sensor and sensor-to-sensor output impedance variations. Still, in the best cases, the cuffless measurement results in a very good match between the sensor and the reference device.

4. Methods

4.1. Fabrication of the P(VDF-TrFE) based ultra-thin e-tattoo PW sensor

First, glass carriers were cleaned and sonicated in deionized (DI) water and soap, DI water, acetone, and isopropanol for 20 min each. Then, a poly(trifluoroethylene) (Teflon, Chemours) dispersion of 1 wt % in FC-40 (Fluorinert, 3 M) was spin-coated on the glass carriers to form a release layer. This process was done to facilitate the separation of the samples from the carriers. 1 g of Parylene-C dimer was then deposited on the glass carrier using chemical vapor deposition (LabTop 3000, Para Tech Coating) in order to fabricate the substrate. The bottom electrode was inkjet printed with a Dimatix Material Printer (DMP-2801, Fujifilm Dimatix) using pristine PEDOT:PSS (Clevios P Jet 700, Heraeus) and PEDOT:PSS mixed with 1 vol % GOPS crosslinker with a 10 pl cartridge, 30 μm drop spacing, two layers while keeping the print platen at room temperature. The electrodes were then annealed for 15 min at 130 °C. This was followed by the deposition of a P(VDF-TrFE) (Ink P, Piezotech Arkema Group) layer on top of the electrodes using an automatic bar coater (Motorized Film Applicator CX4, MTV Messtechnik). The P(VDF-TrFE) was then annealed at 145 °C for 1 h in a convection oven followed by slow cool down to room temperature. The top electrode was fabricated using otherwise same materials/process as for the first electrode layer, but reduced annealing temperature of 100 C. The overlapping area of the top/bottom electrodes was 1 cm^2. To connect the sensor to external devices, thin metal cables were attached to the printed electrodes using flexible PEDOT:PSS screen printing ink (Heraeus STAB) which was cured at 100 °C for 60 min. Finally, the poling process was performed to activate the piezoelectric properties of the P(VDF-TrFE) layer. This was done using the ferroelectric characterization tool (aixACCT TF2000, aixACCT Systems GmbH) coupled with a high-voltage amplifier (610 C, TREK) while doing the polarization-electric (PE) field hysteresis loops measurements.

For PW-measurements, the sensor was removed from the glass carrier by pressing a slightly wetted temporary tattoo paper on top of it while heating the stack to 60 °C for 5 min. This was followed by peeling the sensor from the glass together with the temporary tattoo paper, attaching temporary tattoo adhesive to the bottom of the sensor, attaching it to the skin, and removing the temporary tattoo paper by wetting it and sliding it off. No skin preparation was needed for obtaining sufficient adhesion of the sensor.

4.2. Sensor dimensions and optical transmission

The thickness of the P(VDF-TrFE) layer was measured using a stylus profilometer (Dektak XT, Bruker). Each sample was scanned from two locations and the average of these two measurements was used as the thickness. The transmittance of the sensor was measured using an UV/VIS spectrophotometer (UV-1900i, Shimadzu) using air as baseline.

4.3. Ferroelectric, piezoelectric and electrical characterization

The polarization-electric field (PE) hysteresis loops and leakage current density was measured using a ferroelectric tester (aixACCT TF2000, aixACCT Systems GmbH) coupled with a 10 kV voltage amplifier (610 C, TREK). In leakage current density measurement, the applied electric field was 40 V/μm and the voltage step and duration were 4 V/μm and 2 s, respectively. In PE-loop measurement, the applied electric field was 90 V/μm and the measurement frequency 2,5 Hz. The PE-loop measurement was repeated with the 90 V/μm field until the increase in Pr value between measurements was less than 0,03 $\mu C/cm^2$.

The normal mode, multiaxial and uniaxial bending mode sensitivity were measured using a setup consisting of an electrodynamically actuated (Mini-Shaker Type 4810, Brüel & Kjaer) circular force probe (diameter 4 mm) with integrated dynamic force reference sensor (209C02, PCB Piezotronics) and static force sensor (ELFS-T3E-20 L Measurement Specialties Inc.) (see Figure S10). The sensor was clamped between the force probe and metal stage while controlling the static pressure using the static force reference sensor (for normal mode and multiaxial mode ~ 100 mmHg). For normal mode, the measurements were done while the sensor was still attached to the glass carrier. For multiaxial measurement, the sensor was removed from the glass carrier and attached to ~5 mm thick PDMS (Sylgard 184) substrates with 1:5, 1:10 and 1:15 curing agent-to-DMS ratio. For uniaxial measurement, the sensors were attached on 125 μm thick PET (Melinex ST506, DuPont) with e-tattoo adhesive and the PET was attached to a custom-made test bench where the distance between the supporting structures was 2 cm; a 4 mm diameter metal cylinder was then placed between the force probe and the PET to spread the pressure uniformly along the length of the bending axis. The sensor output was amplified using a charge amplifier while the amplifier and dynamic reference sensor output were transmitted to PC. MATLAB-based signal processing was used to cancel noise, baseline variations and to fit sinusoidal functions to the smoothed sensor and dynamic reference force sensor signal output. Comparison of the sinusoidals resulted in determination of normal mode, uniaxial and multiaxial bending mode sensitivity. The measurement was repeated 5 times for each dynamic force.

The capacitance of the sensors was measured with a semiconductor analyzer (B1500A, Keysight) at 1 kHz frequency, 2 V bias and 50 mV amplitude. The measurement was repeated 10 times for each sensor.

4.4. Arterial pulse wave measurement

Arterial pulse wave measurements were conducted in the supine position for seven voluntary test subjects having no previous history of cardiovascular diseases (see Figure S12). Under the ethical guidelines of Tampere University, measurements done on the participating researchers (i.e. authors of the manuscript) do not require ethical approval. The proposed e-tattoo sensor was attached to the skin on the top of the pulsating radial artery at the distal antebrachium of the left upper limb. A 3-minute period of the signal was recorded in each case with the biasing force provided with ~4 mm thick PDMS sheets having mixture ratios of 1:5, 1:10, and 1:15 and an elastic wristband as well as without any structures providing the bias force. The sensor was connected to a high-input-impedance unity-gain pre-amplifier cascaded with a non-inverting variable-gain amplifier. The amplified sensor signal was sampled with Finapres NOVA (Finapres Medical Systems BV, Netherlands) device, which was also used to collect the reference pulse wave signal, i.e. continuous non-invasive blood pressure measured with a cuff around the left index finger and using the volume-clamp method. The sampling frequencies for the e-tattoo sensor and finger cuff signals were 1 kHz and 200 Hz, respectively.

The e-tattoo sensor signals were low-pass filtered as proposed in [41]. The amplitude-normalized pulse waveforms from both reference signal and e-tattoo sensor signals were synchronized based on their peak points. The peak-point-synchronized pulse waveforms were averaged for visual comparison as well as for radial augmentation index (rAIx) (Fig. 4d) [6,7,41] computation. The agreement between the paired rAIx values based on the reference and the e-tattoo sensor was statistically tested using the 2-tailed Wilcoxon signed-rank test.

CRediT authorship contribution statement

M.M.L.: fabricated the sensors, designed the experiments, analyzed the data and was the primary author of the paper. M.P.: designed the pulse wave measurement experiment, analyzed the pulse wave signals, contributed to the writing of the paper. K.L.M.: assisted with sensor fabrication/characterization, analyzed the transmittance data, contributed to manuscript review. J.V.: designed the amplifiers used in pulse wave measurement, contributed to manuscript review. M.H.: contributed to manuscript review. N.O.: contributed to manuscript review. A. V.: contributed to design of experiment, data analysis and manuscript review. M.M. contributed to design of experiment, data analysis and manuscript review.

Declaration of Competing Interest

The authors declare that they have no known competing financial interests or personal relationships that could have appeared to influence the work reported in this paper.

Data Availability

The datasets generated and analyzed during the current study are available from the corresponding author on reasonable request.

Acknowledgements

This work made use of the Health and Assistive Technology (HeAT) laboratory at Tampere University. The authors would also like to thank Dr. Suvi Lehtimäki at Tampere University for the transmittance measurements. K.L.M would like to thank Tuula and Yrjö Neuvo Fund for support. M.H. would like to thank The Finnish Cultural Foundation for funding. This work was supported by the Academy of Finland under Grant 310617 and Grant 310618. The research used Research Infrastructures “Printed Intelligence Infrastructure” (PII-FIRI, Academy of Finland Grant 320019).

Appendix A. Supporting information

Supplementary data associated with this article can be found in the online version at doi:10.1016/j.nanoen.2022.107625.

References

[1] R. Lozano, et al., Global and regional mortality from 235 causes of death for 20 age groups in 1990 and 2010: a systematic analysis for the Global Burden of Disease Study 2010, Lancet vol. 380 (9859) (2012) 2095–2128.
[2] M.F. O'Rourke, et al., Mechanical factors in arterial aging: a clinical perspective, J. Am. Coll. Cardiol. vol. 50 (1) (2007) 1–13.
[3] M.F. O'Rourke, et al., Pulse wave analysis, Br. J. Clin. Pharmacol. vol. 51 (6) (2001) 507–522.
[4] K. Wilson, et al., Comparison of brachial artery pressure and derived central pressure in the measurement of abdominal aortic aneurysm distensibility, Eur. J. Vasc. Endovasc. Surg. vol. 22 (4) (2001) 355–360.
[5] S. Nandlall, et al., Monitoring and staging Abdominal Aortic Aneurysm (AAA) disease with Pulse Wave Imaging (PWI), Ultrasound Med Biol. vol. 40 (10) (2014) 2404–2414.
[6] J.D. Cameron, et al., Use of radial artery applanation tonometry and a generalized transfer function to determine aortic pressure augmentation in subjects with treated hypertension, Journ. Am. Coll. Card. vol. 32 (5) (1998) 1214–1220.
[7] C. Dagdeviren, et al., Conformable amplified lead zirconate titanate sensors with enhanced piezoelectric response for cutaneous pressure monitoring, Nat. Comm. vol. 5 (2014) 4496.
[8] C. Pang, et al., Highly skin-conformal microhairy sensor for pulse signal amplification, Adv. Mat. vol. 27 (4) (2015) 634–640.
[9] N. Luo, et al., Flexible piezoresistive sensor patch enabling ultralow power cuffless blood pressure measurement, Adv. Funct. Mat. vol. 26 (8) (2016) 1178–1187.
[10] D.Y. Park, et al., Self-powered real-time arterial pulse monitoring using ultrathin epidermal piezoelectric Sensors, Adv. Mat. vol. 29 (37) (2017) 1702308.
[11] C. Wang, et al., Monitoring of the central blood pressure waveform via a conformal ultrasonic device, Nat. Biom. Eng. vol. 2 (2018) 687–695.
[12] S. Gong, et al., Local crack-programmed gold nanowire electronic skin tattoos for in-plane multisensor intergration, Adv. Mat. vol. 31 (41) (2019) 1903789.
[13] K. Sel, et al., Electrical characterization of graphene-based e-tattoos for bio-impedance-based physiological sensing, 2019 IEEE BioCAS Conf. (2019) 1–4.
[14] T. Jin, et al., Ultrathin nanofibrous membranes containing insulating microbeads for highly sensitive flexible pressure sensors, ACS Appl. Mat. Int. vol. 12 (11) (2020) 13348–13359.
[15] A. Petritz, et al., Imperceptible energy harvesting device and biomedical sensor based on ultraflexible ferroelectric transducers and organic diodes, Nat. Commun. vol. 12 (2021) 2399.
[16] J. Wu, et al., A lightweight, ultrathin aramid-based flexible sensor using a combined inkjet printing and buckling strategy, Chem. Eng. Journ. vol. 421/1 (p. 129830) (2021).
[17] K. Lozano Montero et al., “Self-powered, ultrathin, and transparent printed pressure sensor for biosignal monitoring “, ACS Appl. Electr. Mat., In review.
[18] T. Sekine, et al., Fully printed wearable vital sensor for human pulse rate monitoring using ferroelectric polymer, Sci. Rep. vol 8 (2018) 4442.
[19] M.-M. Laurila, et al., Evaluation of printed P(VDF-TrFE) pressure sensor signal quality in arterial pulse wave measurement, IEEE Sens. J. vol. 19 (23) (2019) 11072–11080.
[20] A. Håkansson, et al., Effect of (3–glycidyloxypropyl)trimethoxysilane (GOPS) on the electrical properties of PEDOT:PSS films, J. Polym. Sci. Part B: Polym. Phys. vol. 55 (10) (2017) 814–820.
[21] Y.-F. Wang, et al., Fully printed PEDOT:PSS-based temperature sensor with high humidity stability for wireless healthcare monitoring, Sci. Rep. vol.10 (2020) 2467.
[22] M. El Mahmoudy, et al., Tailoring the electrochemical and mechanical properties of PEDOT:PSS Films for bioelectronics, Macromol. Mater. Eng. vol. 302 (5) (2017) 1600497.
[23] Y. Wang, et al., Low-cost, μm-thick, tape-free electronic tattoo sensors with minimized motion and sweat artifacts NPJ Flex, Electr vol. 2 (2018) 6.
[24] S. Divya, et al., Study on the enhancement of ferroelectric β phase in P(VDF-HFP) films under heating and poling conditions, Eur. Polym. J. vol. 88 (2017) 136–147.
[25] Z. Chen, et al., The conduction mechanism of large on/off ferroelectric diode currents in epitaxial, J. Appl. Phys. vol. 113 (2013), 184106.
[26] G.T. Wright, Space-charge limited currents in insulating materials, Nature vol. 182 (1958) 1296–1297.
[29] "Piezoelectric Transducers for Vibration Control and Damping: Fundamentals of Piezoelectricity: Appendix", Advances in Industrial Control. Springer, London, 2006.
[30] K. Omote, et al., Temperature dependence of elastic, dielectric, and piezoelectric properties of “single crystalline’’ films of vinylidene fluoride trifluoroethylene copolymer, J. Appl. Phys. vol. 81 (1998) 2760.
[31] C. Zweben et al., "Test Methods for Fiber Tensile Strength, Composite Flexural Modulus, and Properties of Fabric-Reinforced Laminates," in Comp. Mat.: Testing and Design (5th Conf.), pp. 228–262, West Conshohocken, PA, 1979.
[32] D.Y. Park, et al., Self-powered real-time arterial pulse monitoring using ultrathin epidermal piezoelectric sensors, Adv. Mat. vol. 29 (37) (2017) 1702308.
[33] S. Rajala, et al., High bending-mode sensitivity of printed piezoelectric poly (vinylidenefluoride-co-trifluoroethylene) sensors, ACS Omega vol. 3 (7) (2018) 8067–8073.
[34] A. Ballato, Piezoelectricity, in: W. Heywang (Ed.), Evolution and Future of a Technology: Basic Material Quartz and Related Innovations, Springer, New York, NY, 2008, pp. 9–35.
[35] P.-H. Ducrot, et al., Optimization Of PVDF-TrFE processing conditions for the fabrication of organic MEMS resonators, Sci. Rep. vol. 6 (2016) 19426.
[36] W. Sim, et al., Theoretical and experimental studies on the parylene diaphragms for microdevices, Microsyst. Technol. vol. 11 (2005) 11–15.
[37] J.S. Eckerle, "Tonometry, Arterial", Encycl. Med. Dev. Instrum., 2006, J.G. Webster (Ed.)., https://doi.org/10.1002/0471732877.emd250.
[38] R.M. Dahan, et al., Structural and electrical properties of PVDF-TrFE/ZnO bilayer and filled PVDF-TrFE /ZnO single layer nanocomposite films, Adv. Mat. Process. Technol. vol. 3 (3) (2017) 300–307.
[39] U. Yaqoob, et al., Effect of surface treated MWCNTs and $BaTiO_3$ nanoparticles on the dielectric properties of a P(VDF-TrFE) matrix, J. Alloy. Comp vol. 695 (2017) 1231–1236.
[40] J.S. Dodds, et al., Piezoelectric characterization of PVDF-TrFE thin films enhanced with ZnO nanoparticles, IEEE Sens. J. vol. 12 (6) (2012) 1889–1890.
[41] K. Takazawa, et al., Underestimation of vasodilator effects of nitroglycerin by upper limb blood pressure, Hypertension vol. 26 (3) (1995) 520–523.